engineering proceedings

MDPI

Proceeding Paper

Sensitivity Analysis-Based Multi-Objective Optimization of an Interior PMSM for Off-Highway Vehicle Applications †

Abd Elkarim Ammar [1,*], Bassem Hichri [2], Simone Musacchio [2], Jean-Daniel Kiefer [2] and Jean-Régis Hadji-Minaglou [1]

[1] Department of Engineering, Faculty of Science, Technology and Medicine (FSTM), University of Luxembourg, L-1359 Luxembourg, Luxembourg; jean-regis.minaglou@uni.lu
[2] CARRARO Lux-Tech-R&D Centre, Mondercange, L-3895 Luxembourg, Luxembourg; bhichri@carrarolux.com (B.H.); smusacchio@carrarolux.com (S.M.); jdkiefer@carrarolux.com (J.-D.K.)
* Correspondence: abd.ammar@uni.lu
† Presented at the 3rd International Electronic Conference on Machines and Applications, 12–14 May 2026; Available online: https://sciforum.net/event/IECMA2026.

Abstract

Off-highway vehicle electrification requires traction motors combining high torque density with reliable performance across demanding duty cycles, yet finite-element-based optimization remains computationally demanding for broad design-space exploration. This study addresses the gap with a sensitivity-analysis-based, surrogate-assisted multi-objective optimization framework for a 12-pole/72-slot, 120 kW Interior Permanent-Magnet Synchronous Motor (IPMSM) for a compact wheel-loader drivetrain, coupling Ansys Motor-CAD with Ansys OptiSLang. A Latin Hypercube sensitivity study of thirteen geometric parameters identifies the dominant design drivers, and an evolutionary algorithm operating on the validated surrogate produces a Pareto-optimal set, from which the final design is selected using the CRITIC–TOPSIS method applied to finite-element-validated feasible designs. Relative to the baseline, the validated performance shows a 7.4% increase in continuous torque, a 4.0% increase in peak torque, a 4.0% increase in efficiency, and a 53.5% reduction in torque ripple, with mass essentially unchanged, while also revealing that surrogate predictions were markedly optimistic relative to the finite-element results. These findings demonstrate an efficient, reliable route to high-performance IPMSM design for off-highway applications.

Keywords: interior permanent magnet synchronous motor (IPMSM); off-highway vehicles; Ansys Motor-CAD; Ansys OptiSLang; surrogate model; evolutionary algorithm; technique for order preference by similarity to an ideal solution (TOPSIS)

Check for updates

Academic Editor: Israel Zamudio-Ramírez

Published: 18 August 2026

Copyright: © 2026 by the authors. Licensee MDPI, Basel, Switzerland. This article is an open access article distributed under the terms and conditions of the Creative Commons Attribution (CC BY) license.

1. Introduction

The electrification of off-highway vehicles has emerged as a major industrial and research priority, driven by tightening emission regulations (EU Stage V, US Tier 4 Final) [1]. Interior Permanent Magnet Synchronous Motors (IPMSMs) are the preferred traction motor topology in this domain due to their high torque density and wide constant-power speed range [2]. The demand for high power density and efficiency in PMSMs requires a solid design approach that cannot rely on traditional analytical methods. Consequently, Finite Element Analysis (FEA) has become the industry standard for designing machine topologies [3]. FEA facilitates a detailed investigation of the air-gap flux density and the nonlinear B-H characteristics of the magnetic materials used in the stator and rotor.

While the finite-element model of the baseline design confirms that the preliminary geometry meets the target performance, it represents only a single point in a much larger design space. A manual exploring the influence of each geometric parameter through repeated finite-element simulations would be computationally prohibitive [4]. A systematic sensitivity analysis is therefore required to identify, among these parameters, the ones that most significantly affect the machine's electromagnetic performance [5].

The choice of sampling method is a key decision that affects both the accuracy of the sensitivity analysis and the quality of the final optimized designs [6]. The number of samples in classical methods like full or fractional factorial grows exponentially with the number of design variables and factor levels. Since each sample corresponds to a computationally expensive operation, this rapid growth leads to high-dimensional simulation problems. Therefore, Latin Hypercube Sampling (LHS) is adopted in the present study as the sampling strategy. LHS decouples the number of samples from the dimensionality of the problem, allowing the computational budget to be fixed a priori while still achieving a near-uniform, space-filling distribution of points across every input dimension [7]. This property makes it possible to construct an accurate metamodel and to derive reliable sensitivity measures from a substantially smaller set of expensive evaluations than classical designs would demand [8].

Despite the fact that FEA provides high electromagnetic accuracy and the sensitivity analysis identifies which geometric parameters strongly influence the performance, these methods require a computationally efficient means of predicting those responses across the design space because each sampled design requires a full finite-element evaluation [9]. Moreover, the direct coupling of an optimization algorithm to the finite-element model would require thousands of additional solver calls. Therefore, a surrogate model is proposed to approximate the FEA model and effectively reduce the computation time [10,11]. An evolutionary optimization algorithm (EA) is therefore employed. It is a population-based method that evolves a set of candidate designs over successive generations through selection, crossover and mutation, evaluating each candidate directly on its objective values rather than requiring gradient information. The evolutionary algorithm implemented in OptiSLang is based on the Strength Pareto Evolutionary Algorithm 2 (SPEA2) [12], which applies elitism through an archive of non-dominated individuals, assigns fitness based on Pareto dominance, and preserves population diversity through density estimation [13].

Beyond the optimization stage itself, selecting a single design from a Pareto-optimal set requires an explicit decision-making step, since no solution is simultaneously the best in every objective. Multi-criteria decision-making (MCDM) methods provide a systematic and reproducible basis for this selection [14]. Among these, the Technique for Order Preference by Similarity to an Ideal Solution (TOPSIS) has been widely applied to electric machine design, ranking candidate designs by their relative distance to an ideal and a non-ideal solution [15]. In Ref. [16], TOPSIS has been used to select the final design from a Pareto front obtained through metamodel-based optimization. The present work adopts the same approach to select the final IPMSM design from the set of finite-element-validated Pareto-optimal candidates.

To address these challenges, this paper presents a surrogate-based optimization framework that couples Ansys Motor-CAD, used for electromagnetic modeling and solving, with Ansys OptiSLang, which drives sensitivity analysis and optimization. The framework is applied to the design of a 120 kW Interior Permanent-Magnet Synchronous Machine (IPMSM) for a wheel-loader drivetrain. A systematic sensitivity analysis of geometric parameters is first performed to identify the most influential design variables. An evolutionary algorithm then carries out optimization on the resulting surrogate model to obtain designs that satisfy all performance targets, and the optimized design is verified against the full finite-element

model. This work builds upon the authors' previous duty-cycle-driven design study [17], in which real-world wheel-loader maneuver analysis was used to derive the torque–speed operating envelope, size a preliminary IPMSM, and characterize its steady-state electromagnetic behavior. The present study differs in both focus and methodology: it concentrates on the systematic design-space exploration through a DoE-based sensitivity analysis and a surrogate model constructed with the Metamodel of Optimal Prognosis, on which a multi-objective evolutionary algorithm employing Pareto-dominance ranking is applied, followed by a TOPSIS selection of the final design from the finite-element-validated Pareto front.

2. Optimization Framework Overview

The overall design and optimization workflow is illustrated in Figure 1. The process begins with the operating requirements derived from the measured duty cycles, which define the target power, torque and speed of the machine. Based on these requirements, preliminary motor sizing is obtained in Ansys Motor-CAD. The design is then transferred to Ansys OptiSLang, where a sensitivity analysis identifies the geometric parameters that most influence the machine responses; a surrogate model is constructed to approximate the finite-element behavior; and then a multi-objective evolutionary algorithm is applied to the surrogate to obtain the model.

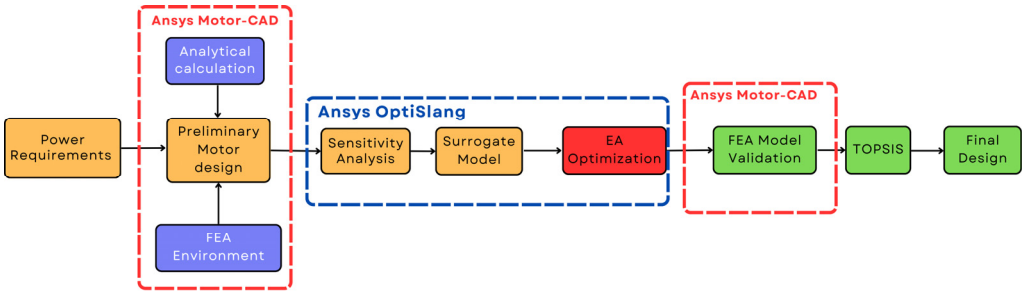


Figure 1. Multi-objective optimization framework.

The optimal designs are subsequently re-evaluated with the full finite-element model in Ansys Motor-CAD. Finally, the validated feasible designs are ranked using the TOPSIS multi-criteria decision-making method, from which the final design is selected.

3. Baseline Motor Model and Power Requirements

3.1. Preliminary Design

The baseline model is a 12-pole, 72-slot Interior PMSM with a V-shaped magnet configuration (Figure 2), designed for a target continuous output power of 120 kW for wheel loader application. The V-shaped rotor topology was selected for its favorable combination of a high saliency ratio and low magnet exposure to demagnetizing fields [18]. The key parameters of the IPMSM are listed in Table 1.

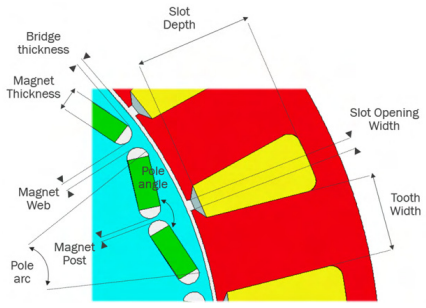


Figure 2. Single pole/slot cross-section of IPMSM with V-shaped magnets.

Table 1. Main parameters of the IPMSM.

Sl. No.	Parameter	Value
1	Pole/Slot configuration	12/72
2	Output power	120 kW
3	Average torque	400 N·m
4	Peak torque (at 2000 rpm)	650 N·m
5	Rated current (RMS)	240 A
6	Stator inner diameter (Di)	232 mm
7	Stator outer diameter (Do)	298 mm

3.2. Duty Cycle Analysis

Heavy-duty off-highway vehicles exhibit significantly more demanding operation than passenger cars, both in the magnitude and the frequency of their power peaks. Rather than relying on standardized driving cycles, the motor requirements in this work are derived from real-world duty cycles measured during actual wheel-loader operation. Two representative operating conditions are used. The Y-cycle, as shown in Figure 3 top, is the most widely adopted representation of the repetitive load-and-carry operation of a wheel loader; it defines the sustained operating demand and forms the basis for the continuous-torque requirement and the duty-cycle average efficiency. The second is the breakout condition at the bottom of Figure 3, which corresponds to the maximum torque required to break out a fully loaded bucket and therefore defines the peak torque requirement.

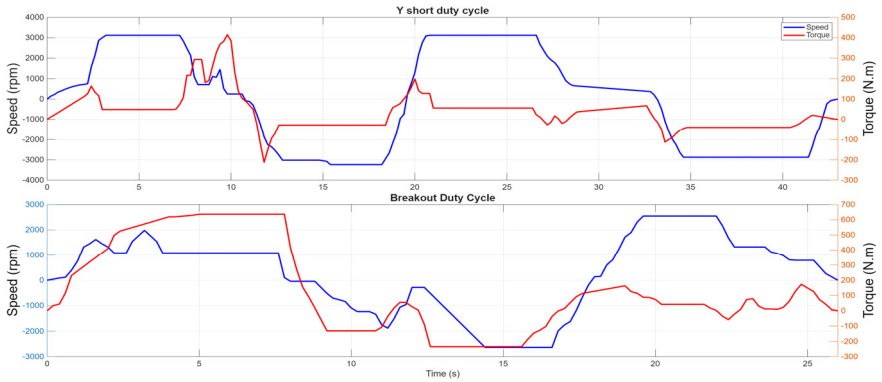


Figure 3. Y-short and breakout duty cycles.

4. Sensitivity Analysis

4.1. Design Parameters and Ranges

The sensitivity analysis targets 13 geometric design parameters that are known from physical reasoning and the prior literature to have significant potential influence on IPMSM electromagnetic performance [9]. Rather than varying all geometric dimensions, the parameter set was restricted to the dimensions that govern the three quantities of interest: torque production, torque ripples, and efficiency. The selected parameters span the stator geometry, the rotor and magnet geometry, and the overall machine sizing. The active stack length and the stator bore ratio set the overall electromagnetic sizing; together they are the primary determinants of torque capability and machine mass. The air-gap length strongly governs the air-gap flux density, and hence, both torque and efficiency. The stator tooth-and-slot geometry controls the winding area; thus, current loading and copper loss are also controlled [19]. On the rotor side, the magnet thickness and V-shape arrangement define the magnet quantity and the flux-focusing geometry, which set the magnet flux linkage, the saliency ratio and, hence, the reluctance torque, and the demagnetization margin [20,21].

The ranges in Table 2 were defined around the baseline design so as to cover the physically meaningful design space while respecting manufacturability and mechanical constraints: dimensional ratios are varied within limits that maintain a viable geometry; the air gap is kept above its minimum feasible value; and the magnet and bridge dimensions are bounded to preserve structural integrity and avoid demagnetization.

Table 2. Design parameters defined for the sensitivity analysis.

Sl. No.	Parameter	Symbol	Baseline	Range
1	Active stack length	L_stack	160 mm	150–260 mm
2	Stator bore ratio	R_bore	0.7785	0.75–0.80
3	Air-gap length	g	1.0 mm	0.7–1 mm
4	Slot depth ratio	R_slot	0.6465	0.60–0.80
5	Tooth width ratio	R_tooth	0.400	0.30–0.40
6	Slot opening ratio	R_open	0.4001	0.40–0.50
7	Tooth tip depth	d_tip	0.5 mm	0.5–1 mm
8	Magnet thickness	t_m	6.0 mm	4.5–6.5 mm
9	Magnet V angle	α_V	150°	120–180°
10	Magnet V width ratio	R_Vw	0.573	0.50–0.60
11	Magnet bar width ratio	R_bw	0.909	0.80–1.00
12	Magnet post width	w_post	0.5 mm	0.5–4.0 mm
13	Bridge thickness	t_bridge	1.0 mm	1.0–3.0 mm

4.2. Objectives and Constraints

The optimization objectives and constraints are defined from the application requirements of the wheel-loader drivetrain. Three objectives are considered (Table 3). The average efficiency of the duty cycle is maximized; the torque ripple is minimized. The total motor mass is minimized to improve power density; it additionally serves as a cost indicator through associated material usage.

Table 3. Design constraints and objectives.

Sl. No	Constraints	Objectives
1	Torque $\geq$ 400 at 3000 rpm	Minimum torque ripples
2	Peak Torque $\geq$ 650 at 2000 rpm	Minimum mass
3	Mass $\leq$ 120 kg	Maximum efficiency

The constraints ensure that the machine meets the operating demands identified from the duty cycles. The continuous torque requirement ($\geq$400 N·m) is derived from the sustained demand of the Y-cycle, and the peak-torque requirement ($\geq$650 N·m) is set by the breakout condition. The total mass is additionally bound by a hard limit corresponding to the power density coefficient.

5. Design Process of Surrogate-Based Optimization

5.1. Sensitivity Test Results

In this study, 100 samples were drawn for the 13-dimensional parameter space, resulting in 100 full FEA evaluations in Ansys Motor-CAD. The sampling stage of the sensitivity analysis was carried out using a Latin Hypercube. LHS was selected because it guarantees uniform coverage of each individual parameter's range while requiring substantially fewer evaluations since each parameter level is sampled exactly once across the design set. Of these 100 successfully evaluated designs, 22 were found to be feasible and they satisfied all performance constraints imposed. Design 81 was selected as the reference design for the

coming steps. The remaining designs were solved correctly; however, if they violated one or more constraints, they were classified as infeasible.

The correlation matrix in Figure 4 relates the geometric input parameters to the five principal machine outputs. The active length emerges as the dominant geometric driver, exhibiting strong positive correlations with the motor weight (r = 0.92) and the peak shaft torque (r = 0.76), consistent with its direct role in scaling active volume and torque. The torque ripple is governed primarily by the magnet V-width ratio (r = 0.66) and, to a lesser extent, the pole V-angle, while the bridge thickness is the only parameter with a notable negative influence, reducing the continuous shaft torque (r = −0.50). The remaining parameters show weak linear correlations ($|r| < 0.2$), indicating that their effect on performance is either minor or predominantly nonlinear.

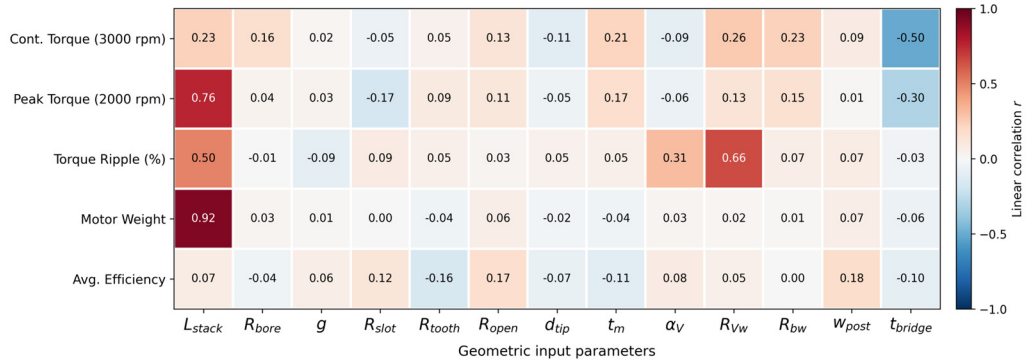


Figure 4. Correlation matrix between the input parameters and the design outcomes.

The linear correlation matrix (Figure 4) captures only linear dependencies between the parameters and the responses. Nonlinear interactions are instead assessed through the Coefficient of Prognosis of the Metamodel of Optimal Prognosis, which is used here as the primary sensitivity measure.

5.2. Surrogate-Based Model

The Metamodel of Optimal Prognosis (MOP) is a data-driven surrogate-modeling approach implemented in Ansys OptiSLang [22]. Unlike classical response-surface methods, which fit a single predefined functional form to the data, the MOP automatically determines each output response independently. The predictive quality of each MOP approximation is quantified by the Coefficient of Prognosis (CoP):

$$CoP = 1 - \frac{SS_{Prediction}}{SS_T} \quad (1)$$

where $SS_{Prediction}$ is the sum of squared prediction errors evaluated at independent points obtained by cross-validation, and SS_T is the total sum of squares of the output response.

A CoP approaching unity indicates near-perfect predictive accuracy, and values above approximately 0.8 are commonly regarded as indicating a metamodel of sufficient quality for reliable optimization.

The candidate library comprises several approximation types, including polynomial regression, Moving Least Squares (MLS), Kriging (Gaussian-process regression) models [23], and deep feed-forward neural networks [24]. In this work, the polynomial regression is set together with a deep feed-forward neural network, allowing the MOP to model responses that cannot be adequately captured by polynomial surfaces alone; for each response, OptiSLang automatically trained and cross-validated both candidates and retained the one with the highest predictive quality. The metamodel is constructed, trained and cross-validated automatically by Ansys OptiSLang using its default configuration; for each

response, the approximation type yielding the highest Coefficient of Prognosis is selected, and the Coefficient of Prognosis is evaluated on data held out from model fitting (cross-validation) rather than on the training residuals.

The total-effect sensitivity indices obtained from the Metamodel of Optimal Prognosis are summarized in Figure 5, where each value represents the share of a response's variance explained by an individual parameter. All five metamodels achieved a high total CoP ranging from 80.1% to 99.0%, confirming that the surrogate models reproduced the solver responses with sufficient accuracy for reliable optimization. The results reveal that each response is governed by a small subset of parameters, while the remaining variables are filtered out (shown in gray) as statistically insignificant.

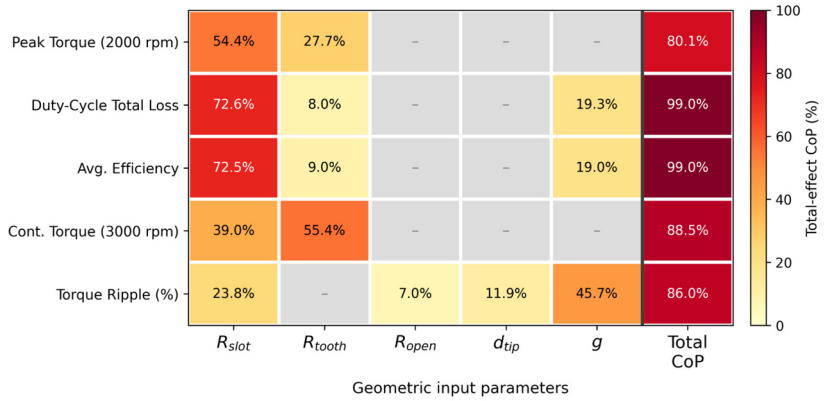


Figure 5. Coefficient of Prognosis of the geometric input parameters.

5.3. EA Optimization

The optimization was performed on the validated Metamodel of Optimal Prognosis using the Evolutionary Algorithm (EA) implemented in Ansys OptiSLang. This evolutionary algorithm is based on the Strength Pareto Evolutionary Algorithm 2 (SPEA2). Because the EA evaluates candidate designs on the surrogate rather than on the full electromagnetic model, up to one thousand designs can be assessed at a negligible computational cost, whereas an equivalent search on the finite-element model would require a prohibitive number of evaluations. This surrogate-based strategy makes a thorough exploration of the design space affordable and yields the estimated Pareto front from which the final design is selected.

Since the design objectives are mutually conflicting, no single solution optimizes all of them simultaneously; the algorithm therefore seeks a set of Pareto-optimal trade-off designs. Design fitness is assessed by Pareto dominance, in which a design is ranked higher when it is no worse in every objective and strictly better in at least one [25]. Constraints are enforced through a rank-order (feasibility-based) scheme, whereby feasible designs are always ranked ahead of infeasible ones, and infeasible designs are ordered by their degree of constraint violation, so the search is driven toward the feasible region without relying on penalty weights [26]. The overall optimization loop is illustrated in Figure 6, and the algorithm settings are summarized in Table 4.

Figure 7 presents the outcome of the multi-objective optimization in the objective plane defined by the total motor weight and the duty-cycle average efficiency. Of the 1000 designs evaluated on the surrogate, 823 are feasible. Figure 7 shows the designs projected onto the mass–torque-ripple plane, spanning a mass range of approximately 70–100 kg; because efficiency is not represented in this projection, the front does not appear strictly monotonic in this plane. Figure 7 shows the three objectives together with the designs subsequently re-evaluated with the full finite-element model in Ansys Motor-CAD. The validated designs (green) are markedly displaced from the surrogate-predicted front,

particularly along the efficiency axis, indicating that the metamodel over-predicted the achievable efficiency and under-predicted the torque ripple relative to the high-fidelity results. This discrepancy confirms the necessity of the full-model validation step: the final design was selected, using the TOPSIS multi-criteria method, from the validated designs rather than from the surrogate-predicted front, ensuring that the reported performance of the final machine reflects genuine finite-element results.

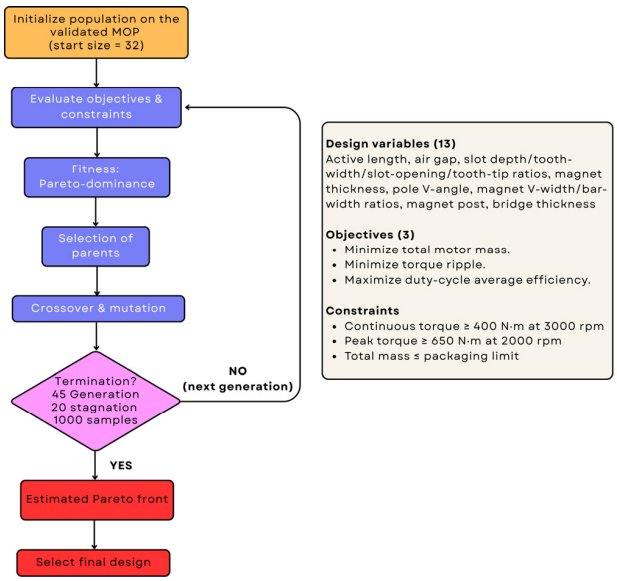


Figure 6. Flowchart of the evolutionary-algorithm optimization performed on MOP.

Table 4. Evolutionary algorithm settings.

Sl. No	Setting	Value
1	Start population size	32
2	Population size	22
3	Maximum number of generations	45
4	Stagnation generations (stopping criterion)	20
5	Maximum number of samples (surrogate evaluations)	1000
6	Fitness method	Pareto dominance

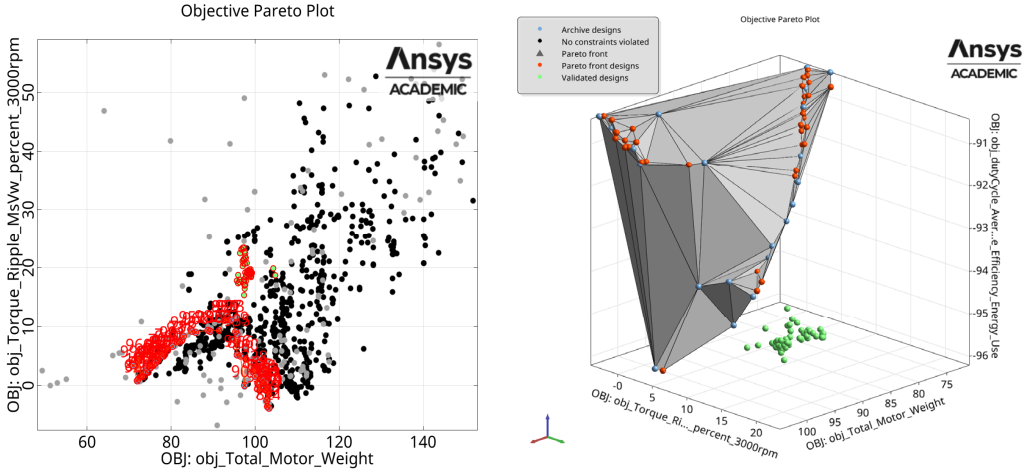


Figure 7. Objective 2D and 3D Pareto plots of the optimized designs.

https://doi.org/10.3390/engproc2026145012

5.4. Final Design Selection

The multi-objective optimization yields a set of Pareto-optimal designs, all of which satisfy the imposed constraints; the selection of a single machine therefore requires an explicit decision step. To place this selection on an objective basis, the Technique for Order Preference by Similarity to an Ideal Solution (TOPSIS) is applied to the feasible Pareto-optimal designs. Surrogate-based optimization is re-evaluated with the full finite-element model in Ansys Motor-CAD. Among 60 re-evaluated designs, 34 satisfied all imposed requirements under a high-fidelity evaluation and constitute the feasible validated set. The final motor is selected from this validated set using TOPSIS, with objective weights obtained by the Criteria Importance Through Intercriteria Correlation (CRITIC) method [16].

For brevity, the ten highest-ranked designs are shown in Table 5; all 34 were included in the ranking.

Table 5. TOPSIS ranking of the feasible Pareto-optimal designs.

Sl. No	Design	Mass (kg)	Ripple (%)	Efficiency (%)
1	983	97.38	15.32	94.632
2	991	97.52	16.42	94.909
3	884	97.49	16.96	94.860
4	982	97.68	17.08	94.960
5	961	97.39	17.64	94.849
6	882	97.90	17.79	94.889
7	813	97.52	17.98	94.800
8	863	97.72	18.35	94.745
9	951	99.05	18.41	94.671
10	979	99.10	18.57	94.775

Table 6 reports the corresponding closeness scores and ranking obtained by applying the CRITIC-weighted TOPSIS method to the ten candidate designs listed in Table 5.

Table 6. TOPSIS closeness scores and ranking of the ten highest-ranked candidate designs.

Sl. No	Design	Mass (kg)	Ripple (%)	Eff (%)	Score	Rank
1	**983**	**97.38**	**15.32**	**94.63**	**0.97402**	**1**
2	991	97.52	16.42	94.91	0.75214	2
3	884	97.49	16.96	94.86	0.63199	3
4	982	97.68	17.08	94.96	0.60362	4
5	961	97.39	17.64	94.85	0.48162	5
6	882	97.90	17.79	94.89	0.44312	6
7	813	97.52	17.98	94.80	0.40060	7
8	863	97.72	18.35	94.75	0.32290	8
9	951	99.05	18.41	94.67	0.29270	9
10	979	99.10	18.57	94.78	0.25710	10

Design 983 is selected as the final machine. Among the validated feasible designs, it attains the lowest torque ripple (15.3%) and one of the lowest masses (97.4 kg), at a duty-cycle average efficiency of 94.6%. Because the validated designs differ only marginally in mass and efficiency, the torque ripple is the decisive criterion, and Design 983 offers the best overall compromise on the validated (finite-element) results.

It should be noted that the validated performance differs from the surrogate prediction: the finite-element efficiency (about 94.6–95.0%) is lower than predicted, and the finite-element torque ripple (about 15–20%) is substantially higher than predicted. This

is consistent with the surrogate approximation error and confirms the necessity of the validation stage. All reported performance values for the final design are given in the validated finite-element results.

Table 7 shows the parameters of the final validated design (Design 983) compared to the baseline and the sensitivity MOP-based design.

Table 7. Design parameters: baseline vs. sensitivity design (81) and EA optimized design (983).

Sl. No	Parameter	Initial Design	Sensitivity 81	EA Optimized 983
1	Active Stack Length	160 mm	176.25 mm	180.96 mm
2	Stator Bore Ratio	0.7785	0.789	0.752
3	Air-Gap Length	1.0 mm	0.89 mm	0.94 mm
4	Slot Depth Ratio	0.6465	0.631	0.641
5	Tooth Width Ratio	0.4	0.3965	0.4
6	Slot Opening Ratio	0.4	0.4545	0.4
7	Tooth Tip Depth	0.5 mm	0.98 mm	0.5 mm
8	Magnet Thickness	6.0 mm	6.19 mm	6.5 mm
9	Pole V Angle	150°	147.9°	129.14°
10	Magnet V Width Ratio	0.573	0.521	0.5
11	Magnet Bar Width Ratio	0.909	0.951	0.89
12	Magnet Post Width	0.5 mm	0.9125 mm	0.55 mm
13	Bridge Thickness	1.0 mm	1.87 mm	1.28 mm

5.5. Final Model Evaluation

Because the evolutionary algorithm evaluates candidate designs on the metamodel rather than on the full electromagnetic model, the selected design is re-evaluated with the full finite-element model in Ansys Motor-CAD as the final step of the workflow. Table 8 compares the metamodel-predicted responses of the selected design with the finite-element results. The final design was selected from the 34 designs confirmed as a feasible model; however, its validated performance differs from the surrogate prediction. All performance values reported for the final design are the validated finite-element results shown in Table 8.

Table 8. Metamodel-predicted VS finite-element (Motor-CAD) results for the selected design.

Sl. No	Response	Baseline Design	Design 983 MOP Prediction	Design 983 FEA (Motor-CAD)	Error
1	Torque (N·m)	419	400.82	450	49.18
2	Peak torque (N·m)	648	651.0756	674.1	23.02
3	Total mass (kg)	97.70	75.76	97.37	21.61
4	Duty-cycle efficiency (%)	90.97	90.96	94.63	3.67
5	Torque ripple (%)	32.91	3.37	15.32	11.95

The continuous torque, peak torque, and duty-cycle efficiency are predicted with relative errors of 10.9%, 3.4%, and 3.9% respectively, indicating that the surrogate reproduces these responses with reasonable accuracy. In contrast, the total motor mass and, most notably, the torque ripple show substantially larger deviations. This pattern indicates that the metamodel is considerably less accurate for the torque-ripple and mass responses than for the torque and efficiency responses, most likely because torque ripple depends on fine, highly nonlinear local variations in the air-gap flux distribution that are more difficult for a global surrogate to capture from a limited sample set. These results confirm the necessity of the full-model validation stage.

6. Conclusions

This paper presented a sensitivity-analysis-based multi-objective optimization framework for a 120 kW Interior PMSM for compact wheel-loader drivetrains, coupling finite-element modeling in Ansys Motor-CAD with surrogate-based sensitivity analysis and optimization in Ansys OptiSLang. A Latin Hypercube sensitivity study assesses thirteen geometric parameters that have a dominant effect on motor performance, such as torque ripples and efficiency. While the Metamodel of Optimal Prognosis reproduced the sampled responses with a Coefficient of Prognosis of 80.1–99.0%, an evolutionary algorithm produced a set of Pareto-optimal designs, which were subsequently re-evaluated with the full finite-element model. The final design was selected using the TOPSIS multi-criteria decision-making method from the designs confirmed feasible under validation.

Compared to the baseline motor, the validated performance of the selected design (No. 983) shows a 7.4% increase in continuous torque, a 4.0% increase in peak torque, a 4.0% increase in duty-cycle efficiency, and a 53.5% reduction in torque ripple, while the total mass remains essentially unchanged. These improvements were confirmed on finite-element-validated results rather than surrogate predictions, which were found to be optimistic, particularly for torque ripple and mass. These results demonstrate that the proposed surrogate-based framework provides an efficient and reliable route to improving the performance of an off-highway traction IPMSM, while highlighting the surrogate's reduced accuracy for torque ripple and mass prediction as a specific target for improved sampling in future work. Future work will integrate thermal and mechanical-stress analyses into the optimization loop.

Author Contributions: Conceptualization, A.E.A. and J.-R.H.-M.; methodology, A.E.A.; software, A.E.A.; validation, A.E.A.; formal analysis, A.E.A.; investigation, A.E.A.; resources, B.H., S.M. and J.-D.K.; data curation, S.M. and B.H.; writing—original draft preparation, A.E.A.; writing—review and editing, J.-R.H.-M., B.H. and S.M.; visualization, A.E.A.; supervision, J.-R.H.-M.; project administration, B.H. and J.-D.K.; funding acquisition, J.-D.K. and J.-R.H.-M. All authors have read and agreed to the published version of the manuscript.

Funding: This research was supported by CARRARO Lux-Tech-R&D Centre within the E-TRANS project, conducted in partnership with the University of Luxembourg.

Data Availability Statement: The data used in this study were provided by CARRARO Lux-Tech-R&D Centre and are subject to confidentiality restrictions. They are not publicly available due to their proprietary and commercially sensitive nature.

Conflicts of Interest: Authors Bassem Hichri, Simone Musacchio and Jean-Daniel Kiefer were employed by the company CARRARO Lux-Tech-R&D Centre. The remaining authors declare that the research was conducted in the absence of any commercial or financial relationships that could be construed as a potential conflict of interest.

References

1. Hagan, R.; Markey, E.; Clancy, J.; Keating, M.; Donnelly, A.; O'Connor, D.J.; Morrison, L.; McGillicuddy, E.J. Non-Road Mobile Machinery Emissions and Regulations: A Review. *Air* **2022**, *1*, 14–36. [CrossRef]
2. Ozer, K.; Yilmaz, M. Design and Optimization of IPMSM for Enhanced Efficiency, Cost Reduction, and Performance in Light Electric Vehicles. *IEEE Access* **2025**, *13*, 80621–80636. [CrossRef]
3. Coteț, F.-A.; Văscan, I.; Szabó, L. On the Usefulness of Employing ANSYS Motor-CAD Software in Designing Permanent Magnet Synchronous Machines. *Designs* **2023**, *7*, 7. [CrossRef]
4. Mohamed, M.Y.; Refaat, A.; Kalas, A.; Abdel-Khalik, A.S.; Ahmed, S.; Fawzi, M. Optimal Design for Six-Phase Asymmetrical Surface Mount Permanent Magnet Synchronous Motor: An Innovative Approach Considering Fault Tolerance and Load Variations for Electric Vehicle Applications. *Heliyon* **2025**, *11*, e42193. [CrossRef] [PubMed]
5. Newman, K.B.; Naha, S.; Jackson-Blake, L.A.; Topp, C.; Glendell, M.; Butler, A. Global Sensitivity Analysis Workflows and Rankings: A Practical Comparison for Researchers. *Environ. Model. Softw.* **2026**, *200*, 106956. [CrossRef]

6. Esenboğa, B. Parametric Sensitivity-Based Optimization of Additively Manufactured Permanent Magnets for Enhanced PMDC Motor Performance. *IEEE Access* **2026**, *14*, 45179–45190. [CrossRef]
7. Chang, H.; Long, F.; Li, J. Fusion of NSGA-II and Latin Hypercube Sampling for Optimizing Node Displacement in Thin-Film IME Molding. *Sci. Rep.* **2026**, *16*, 9026. [CrossRef] [PubMed]
8. Asef, P.; Denai, M.; Paulides, J.J.H.; Marques, B.R.; Lapthorn, A. A Novel Multi-Criteria Local Latin Hypercube Refinement System for Commutation Angle Improvement in IPMSMs. *IEEE Trans. Ind. Appl.* **2023**, *59*, 1588–1602. [CrossRef]
9. Song, T.; Zhang, Z.; Liu, H.; Hu, W. Multi-objective Optimisation Design and Performance Comparison of Permanent Magnet Synchronous Motor for EVs Based on FEA. *IET Electr. Power Appl.* **2019**, *13*, 1157–1166. [CrossRef]
10. Yu, Y.; Liang, C.; Zeng, D.; Hu, Y.; Yang, J. Multi-Objective Optimization of IPMSM for Electric Vehicles Based on the Combinatorial Surrogate Model and the Hierarchical Design Method. *Int. J. Electr. Power Energy Syst.* **2024**, *162*, 110245. [CrossRef]
11. Lee, S.-C.; Kang, D.H.; Jung, S.-W.; Jung, S.-Y. Hybrid Sampling Strategies for a Surrogate Model in High-Dimensional Space for Electric Motor Design. *J. Electr. Eng. Technol.* **2026**, *21*, 449–463. [CrossRef]
12. Sheng, W.; Liu, Y.; Meng, X.; Zhang, T. An Improved Strength Pareto Evolutionary Algorithm 2 with Application to the Optimization of Distributed Generations. *Comput. Math. Appl.* **2012**, *64*, 944–955. [CrossRef]
13. Beniakar, M.E.; Kakosimos, P.E.; Kladas, A.G. Strength Pareto Evolutionary Optimization of an In-Wheel PM Motor with Unequal Teeth for Electric Traction. *IEEE Trans. Magn.* **2015**, *51*, 8102804. [CrossRef]
14. Taherdoost, H.; Madanchian, M. Multi-Criteria Decision Making (MCDM) Methods and Concepts. *Encyclopedia* **2023**, *3*, 77–87. [CrossRef]
15. Feng, L.; Liu, W.; Ding, Y.; Li, H. Optimal Design and Analysis of High-Speed Permanent Magnet Synchronous Motor Based on Genetic Algorithm and TOPSIS Method. *J. Electr. Eng. Technol.* **2025**, *20*, 1463–1473. [CrossRef]
16. Ye, X.; Zeng, Q.; Sun, R.; Zhang, T. Torque Optimization Strategy for Outer Rotor Permanent Magnet Brushless DC Motor Based on Metamodel and CRITIC–TOPSIS Method. *Electr. Eng.* **2025**, *107*, 1643–1658. [CrossRef]
17. Ammar, A.E.; Hichri, B.; Musacchio, S.; Kiefer, J.; Hadji-Minaglou, J.-R. Design And Optimization of An Interior PMSM For Off-Highway Vehicle Application Based on Real World Manoeuvre Analysis. In Proceedings of the 15th International Conference on Power Electronics, Machines and Drives (PEMD Global 2026), London, UK, 13–15 April 2026.
18. Wang, S.C.; Nien, Y.C.; Huang, S.M. Multi-Objective Optimization Design and Analysis of V-Shape Permanent Magnet Synchronous Motor. *Energies* **2022**, *15*, 3496. [CrossRef]
19. Niu, L.; Zhang, M. The Optimal Design and Research of Interior Permanent Magnet Synchronous Motors for Electric Vehicle Applications. *J. Eng.* **2023**, *2023*, e12258. [CrossRef]
20. Zhou, K.; Wang, D.; Yu, Z.; Yuan, X.; Zhang, M.; Zheng, Y. Strength Analysis and Design of a Multi-Bridge V-Shaped Rotor for High-Speed Interior Permanent Magnet Synchronous Motors. *Actuators* **2025**, *14*, 69. [CrossRef]
21. Zhang, G.; Jewell, G.W. Combined Electromagnetic and Mechanical Design Optimization of Interior Permanent Magnet Rotors for Electric Vehicle Drivetrains. *World Electr. Veh. J.* **2024**, *15*, 4. [CrossRef]
22. Ansys Inc. *OptiSLang User 's Guide*; Ansys, Inc.: Canonsburg, PA, USA, 2024.
23. Lee, Y.-M.; Ko, D.-H.; Park, M.-R. Comparative Study of Kriging and Deep Neural Networks as Surrogate Models for Parameter Prediction of PMSM. *Int. J. Automot. Technol.* **2026**. [CrossRef]
24. LeCun, Y.; Bengio, Y.; Hinton, G. Deep Learning. *Nature* **2015**, *521*, 436–444. [CrossRef] [PubMed]
25. Sun, C.; Li, Q.; Fan, T.; Wen, X.; Li, Y.; Li, H. Multi-Objective Optimal Design of 200 KW Permanent Magnet Synchronous Motor Based on NSGA-II. *World Electr. Veh. J.* **2025**, *16*, 299. [CrossRef]
26. Rahimi, I.; Gandomi, A.H.; Chen, F.; Mezura-Montes, E. A Review on Constraint Handling Techniques for Population-Based Algorithms: From Single-Objective to Multi-Objective Optimization. *Arch. Comput. Methods Eng.* **2023**, *30*, 2181–2209. [CrossRef]

Disclaimer/Publisher's Note: The statements, opinions and data contained in all publications are solely those of the individual author(s) and contributor(s) and not of MDPI and/or the editor(s). MDPI and/or the editor(s) disclaim responsibility for any injury to people or property resulting from any ideas, methods, instructions or products referred to in the content.